SCIENTIFIC REPORTS

OPEN

SUBJECT AREAS:
LAB-ON-A-CHIP
BIOSENSORS
ISOLATION, SEPARATION AND PURIFICATION
ASSAY SYSTEMS

Received
20 October 2014

Accepted
9 December 2014

Published
12 January 2015

Correspondence and requests for materials should be addressed to S.J. (jeons@postech.ac.kr)

3D-Printed Microfluidic Device for the Detection of Pathogenic Bacteria Using Size-based Separation in Helical Channel with Trapezoid Cross-Section

Wonjae Lee[1], Donghoon Kwon[1], Woong Choi[2], Gyoo Yeol Jung[2] & Sangmin Jeon[1]

[1]Department of Chemical Engineering, Pohang University of Science and Technology (POSTECH), Pohang, Gyeongbuk, Republic of Korea, [2]School of Interdisciplinary Bioscience and Bioengineering, Pohang University of Science and Technology (POSTECH), Pohang, Republic of Korea.

A facile method has been developed to detect pathogenic bacteria using magnetic nanoparticle clusters (MNCs) and a 3D-printed helical microchannel. Antibody-functionalized MNCs were used to capture E. coli (EC) bacteria in milk, and the free MNCs and MNC-EC complexes were separated from the milk using a permanent magnet. The free MNCs and MNC-EC complexes were dispersed in a buffer solution, then the solution was injected into a helical microchannel device with or without a sheath flow. The MNC-EC complexes were separated from the free MNCs via the Dean drag force and lift force, and the separation was facilitated in the presence of a sheath flow. The concentration of the E. coli bacteria was determined using a light absorption spectrometer, and the limit of detection was found to be 10 cfu/mL in buffer solution and 100 cfu/mL in milk.

Foodborne diseases commonly caused by pathogenic bacteria are vital concerns to public health worldwide. Because bacteria proliferate over time, sensitive detection of bacteria at early stage is critical for preventing food-borne diseases[1]. Conventional detection methods based on microbial cultivation are accurate and reliable, and considered to be golden standard methods. However, they are time-consuming and labor-intensive, so their application is limited to laboratory measurements[2]. Several methods for rapid detection of bacteria without cultivation have been reported including polymerase chain reaction (PCR)[3,4], quartz crystal microbalance (QCM)[5,6], surface plasmon resonance (SPR)[7,8], electrochemical impedance spectroscopy (EIS)[9], surface-enhanced Raman scattering (SERS)[10,11], and fluorescence spectroscopy[12]. However, they still require complex pretreatment procedures to separate bacteria from food matrices.

This need for complex pretreatment may be mitigated by adopting immunomagnetic assays that use antibody-functionalized magnetic nanoparticles to capture and separate bacteria from food matrices under an external magnetic field. To determine the concentration of bacteria, conventional immunomagnetic assays label captured bacteria with fluorescent molecules or quantum dots to distinguish the bacteria-magnetic nanoparticle complexes from free magnetic particles[13–15]. Size-based separation techniques are good alternative approaches which do not require a complicated labeling procedure. For instance, larger bacteria-magnetic nanoparticle complexes are easily separated from smaller free magnetic nanoparticles using filter membranes[16]. However, filtration has a drawback of a high background noise due to inefficient separation of free magnetic nanoparticles, which degrades the detection sensitivity.

Instead of the use of filter membranes, size-based microfluidic separation methods have been reported for isolation of red blood cells[17], circulating tumor cells[18], and microparticles[19]. Among the microfluidic separation methods such as surface acoustic waves[20], inertial focusing[21] and deterministic lateral displacement[22], the inertial focusing method based on Dean drag force has attracted much attentions because it is easy to control the operation condition with no external force and small chance of physically damaging the cells during separation. Cells or particles can be separated by inertial focusing using spiral microchannels fabricated in a two-dimensional PDMS substrate[23–25]. However, in a spiral channel on a flat substrate, the radius of curvature changes; therefore its Dean number changes, so the flow behavior is difficult to predict and separation is hard to control.

In this paper, we used stereolithography[26,27] to fabricate a helical microchannel around a cylindrical chamber. The vertically designed device offers a constant radius of curvature and compact size. We applied the 3D-printed microfluidic device for rapid and facile detection of *E. coli* (EC) bacteria in a real food matrix. After the capture of *E. coli* bacteria in milk using antibody-functionalized magnetic nanoparticle clusters (MNCs), the free MNCs and MNC-EC complexes were separated using the 3D helical microchannel device. Combined with UV-vis spectroscopy, our method could detect the presence of pathogenic bacteria in 10 mL of a milk sample with a sensitivity of 100 cfu/mL (colony-forming units per mL). The separation was verified by using dynamic light scattering (DLS) and ATP luminescence measurements. Selectivity of the assay was tested against Salmonella typhimurium and Staphylococcus aureus bacteria, and we verified that this detection method can capture and isolate desired target only.

Results and Discussion

Characterization of the MNCs and MNC-EC complexes. Figure 1(a) and 1(b) show a scanning electron microscopy (SEM) image of free MNCs and a transmission electron microscopy (TEM) image of a MNC-EC complex, respectively. The average size of the MNCs was approximately 150 nm, and each consisted of a few hundred 15 nm Fe_3O_4 nanoparticles. The large size of MNC promotes more effective magnetic separation from the analyte compared to small Fe_3O_4 nanoparticles because the magnetic force experienced is proportional to the volume of a particle. An *E. coli* bacterium is about one order of magnitude larger than an MNC and this size difference is the main driving force to separate EC-MNC complexes from free MNCs under the conditions of helical flow.

Design principle and characterization of the MNCs. Figure 2(a) shows the 3D CAD design of the device and the separation scheme for isolating MNC-EC complexes. A sample solution containing free MNCs and MNC-EC complexes is injected into the outer inlet of the device. A sheath flow, if needed, is injected into the inner inlet of the device. When a fluid passes through a curved microchannel, secondary flow that consist of two vortices is generated (Figure 2(b)). These vortices are known as Dean vortices, and their magnitude can be expressed by using the dimensionless Dean number (*De*) and Dean drag force (F_D)[28],

$$De = \frac{\rho U_f D_h}{\mu}\sqrt{\frac{D_h}{2R}} \quad (1)$$

$$F_D = 5.4\times10^{-4}\pi\mu De^{1.63}a_p \quad (2)$$

where ρ is density, U_f is fluid velocity, D_h is hydraulic diameter, μ is dynamic viscosity, R is the radius of curvature of the channel, and a_p is the hydrodynamic diameter. Because *De* is inversely proportional to the radius of curvature and because the magnitude of F_D experienced by the particle increases with the increasing a_p and *De*, separation of particles with two different sizes can be facilitated by increasing the size difference between particles and by using a helical channel with small radius of curvature. In addition to F_D parallel to the Dean flow direction, the particles in a fluid flow also experience a lift force F_L perpendicular to the primary flow direction. F_L can be expressed as a function of particle size and particle position across the channel cross-section[29].

$$F_L = \rho G^2 C_L a_p{}^4 \quad (3)$$

where G is the fluid shear rate and C_L (assumed to be 0.5)[21] is the lift coefficient as a function of the particle position across the channel cross-section. Because the MNC-EC complexes are one order of magnitude larger than the free MNCs, F_D and F_L have significantly stronger effect on MNC-EC complexes than on free MNCs, enabling separation of MNC-EC complexes from free MNCs. The velocity of the fluid varies within the channel cross-section, so the magnitude and direction of both F_D and F_L also vary as a function of the particle's relative position. As a result, large particles become focused at the equilibrium position near the inner wall of the microchannel where F_D and F_L are balanced.

To enhance the effectiveness of separation, the microchannel was designed to have a trapezoidal cross-section, and an additional inlet was added to the device to allow injection of a sheath flow. The asymmetric nature of the trapezoidal channel cross-section (Fig 2(b)) induces strong Dean vortex cores to form close to the outer wall and traps smaller particles within the cores[30]. The sheath flow was used to induce initial focusing of both free MNCs and MNC-EC complexes towards the outer wall of the microchannel. After the sample was passed through the helical microchannel, the size-sorting effect of F_D and F_L caused only the MNC-EC complexes to migrate towards the inner wall. Figure 2(c) shows the photographic image of 3D-printed microfluidic device used in this study. The fabricated device incorporated 10 loops of helical microchannel to provide sufficient length needed for particle migration[31]. The width of the trapezoidal channel cross-section was 1000 μm, and the inner and outer heights were 250 μm and 500 μm, respectively. Such dimensions were determined by the minimum resolution of the 3D-printer used for fabrication of the device, and the experimental results exhibited satisfying performance of the device. The inlet and outlet are in the same plane. However, the inlet is connected to the top of the helix with a vertical channel. The reason that the inlet is not in above plane is to avoid overhang structure which is not favorable for 3D-printing. The inlets and outlets were connected with tubing by barbed luer lock connectors to provide easy tight seal and prevent leakage.

MNC separation performance of the device. The MNC separation performance of the microfluidic device with or without the sheath flow was characterized using DLS measurements. To evaluate the effectiveness of separation without the sheath flow, only one inlet was used; the other inlet was sealed with a luer cap. A sample containing free MNCs and MNC-EC complexes (obtained from

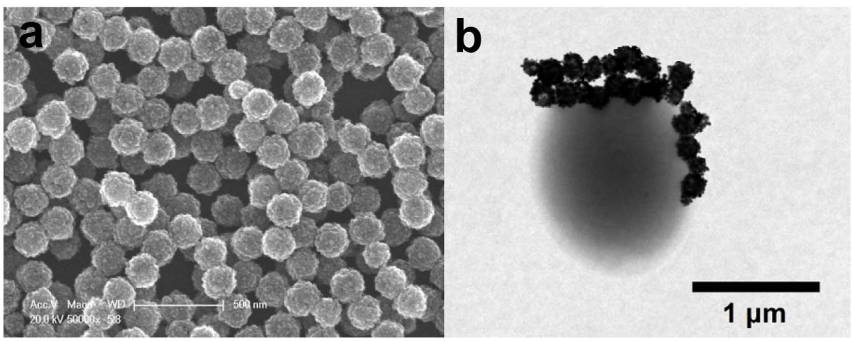

Figure 1 | (a) SEM image of MNCs, (b) TEM image of an MNC-EC complex.

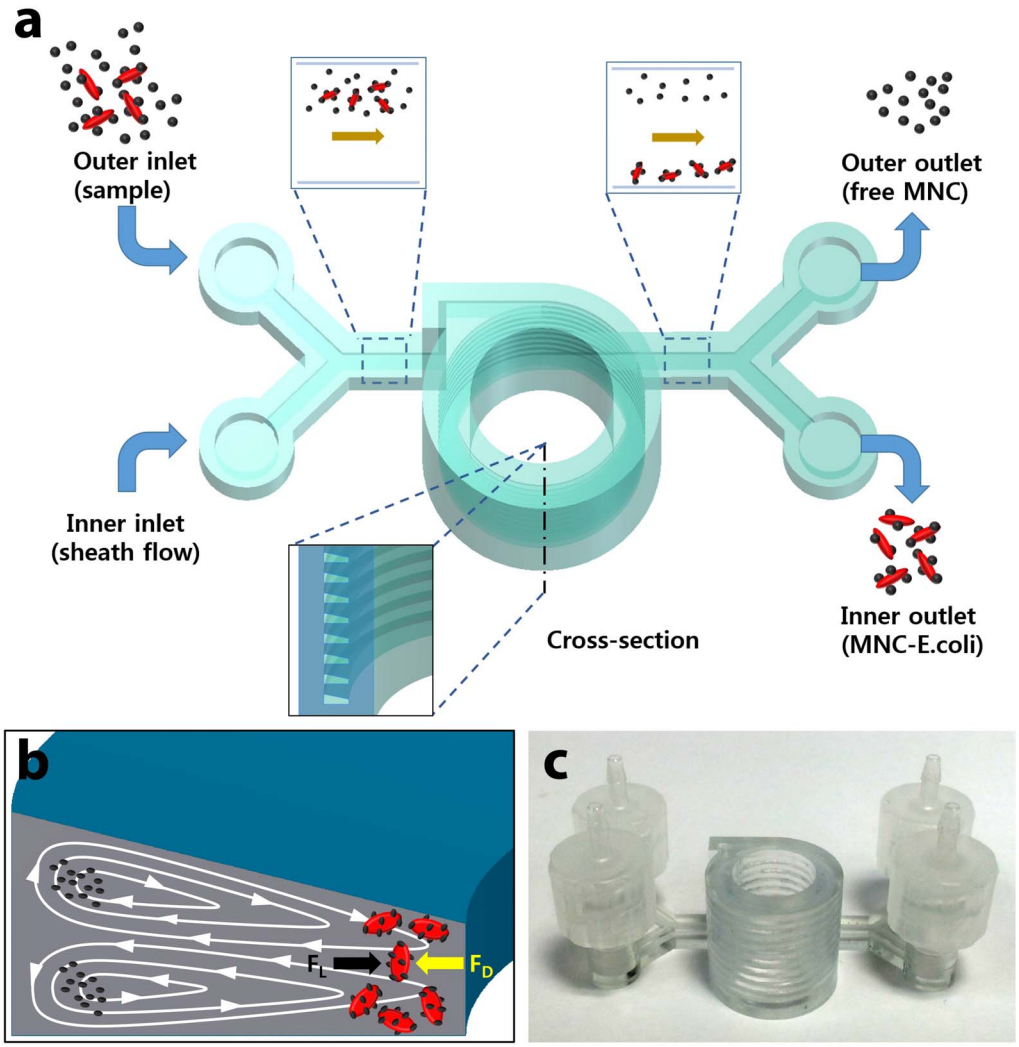

Figure 2 | (a) Schematic illustration of separation of captured bacteria by inertial focusing. (b) Illustration of Dean vortices in a channel with trapezoid cross-section. (c) Photograph of the 3D printed device.

milk spiked with 10^5 cfu/mL *E. coli*) in 5 mL of buffer solution was introduced into the separator at the flow rate of 10 mL/min, and the size distribution of the collected samples from each outlet was measured using DLS.

Figure 3(a) shows the number mean size distribution of the sample solution before passing through the device. The two peaks at 150 nm and 1020 nm correspond to free MNCs and MNC-EC complexes, respectively. The peak amplitude at 150 nm is bigger than the one at 1020 nm because the concentration of free MNCs are much higher than that of MNC-EC complexes. The peak at 1020 becomes more conspicuous in the intensity mean size distribution shown in the inset of Figure 3(a) because the scattering intensity is proportional to the sixth power of the particle diameter. After the inlet solution was passed through the microchannel and divided into two outlet solutions, the size distribution curves were obtained for both the inner outlet and outer outlet solutions. The sample solution from the outer outlet showed only one peak at 150 nm (Figure 3(b)), which corresponds to free MNCs and indicates that no MNC-EC complexes were present in this solution. However, the inner outlet solution showed two peaks (Figure 3(c)), which implied that the separation was not successful and both free MNCs and MNC-EC complexes remained in the solution. The incomplete separation of particles was attributed to the fact that the free MNCs that were initially distributed randomly throughout the entire inlet area were too small to be migrated by Dean drag force under the experimental conditions.

To improve the separation, a sheath flow was introduced into the inner inlet of the separator. The sheath flow pushes the particles to the outer wall side of the microchannel and helps their trapping in the strong Dean vortex cores. The solution obtained from *E. coli*-spiked buffer solution (10^5 cfu/mL) was injected into the outer inlet of the separator at 5 mL/min and the sheath flow was injected into the inner inlet of the separator at 5 mL/min (10 mL/min in total). The sheath flow was injected at the same flow rate as the sample flow because the outlet is bifurcated evenly; slower sheath flow would not push the particles towards outer wall beyond the center line of the channel, and faster sheath flow would significantly dilute the sample. In contrast to the incomplete separation without the sheath flow, complete separation was achieved when the sheath flow was provided. The single peak in Figure 4(a) and 4(b) obtained from the inner outlet and outer outlet solutions corresponds to MNC-EC complexes and free MNCs, respectively.

Detection of *E. coli*. After separation of the MNC-EC complexes from the free MNCs, the concentration of *E. coli* was measured using a portable UV-vis spectrometer. Figure 5(a) and 5(b) show the light absorption spectra for the inner outlet solutions after the injection of various concentrations of *E. coli* in buffer and milk, respectively. The light absorbance intensity increased with the concentration of *E. coli* in both buffer and milk solutions. The peak absorbance intensity was observed at 484.9 nm. Figure 5(c) and 5(d) show variations in the

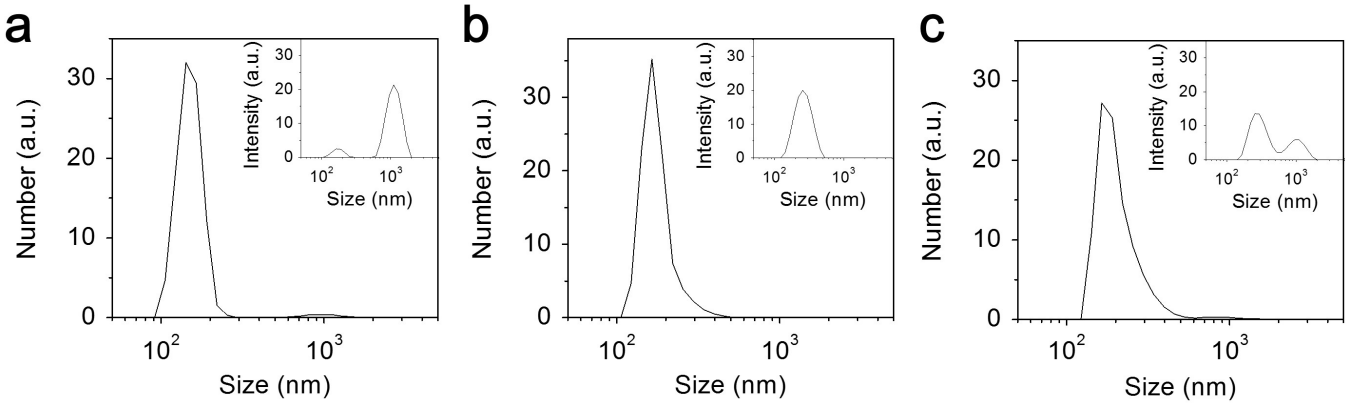

Figure 3 | DLS number mean size distribution curves of the solution (a) at the inlet, (b) at the outer outlet, and (c) at the inner outlet in case of no sheath flow input. Intensity mean size distribution curves are shown as insets. No separation of particles was observed.

light absorbance intensity at 484.9 nm with the concentration of *E. coli* buffer and milk, respectively. The detection limit was found to be 10 cfu/mL for buffer samples and decreased to 100 cfu/mL for milk samples due to the less efficient capture process by the presence of interferents.

Verification of MNC-EC complexes using a portable ATP luminometer. An ATP luminometer was used to verify that the separated samples obtained at the inner outlet were MNC-EC complexes. Because luminescence emission occurs only in the presence of living organisms containing ATP, the intensity of luminescence is directly related to the concentration of *E. coli*. After separating MNC-EC from sample solutions with various concentrations of *E. coli* bacteria in milk, the ATP luminescence for samples from each outlet was measured. Figure 6(a) shows that the luminescence signal was detected only from the inner outlet, confirming that the separation was successful. The limit of detection was found to be better than 100 cfu/mL, which is comparable to the results from light absorption measurements. The selectivity of the detection assay was examined using control samples of 10 mL milk solution spiked with 10^5 cfu/mL *Salmonella* bacteria or *Staphylococcus* bacteria. After incubation of *E. coli* antibody-functionalized MNCs in the control sample, the detection assay was conducted and the luminescence intensity was measured. As shown in Figure 6(b), the signal intensities from the samples containing *Salmonella* bacteria or *Staphylococcus* bacteria were lower than the noise level, indicating that nonspecific binding was negligible.

Conclusions

In summary, we have demonstrated a facile method to detect pathogenic bacteria using an immunoassay in combination with a 3D-printed helical microchannel device. After *E. coli* bacteria in milk was captured using antibody-functionalized MNCs, the free MNCs and MNC-EC complexes were separated by the 3D-printed microfluidic device based on the size difference between the particles. The detection limit of the assay for *E. coli* bacteria-spiked sample solutions was evaluated by UV-Vis absorption spectroscopy and found to be 10 cfu/mL in buffer and 100 cfu/mL in milk. Further, incorporation of 3D-printing technology enabled easy development of a microfluidic device with complex structures to facilitate the effective and efficient detection of pathogenic bacteria on site.

Methods

Materials. Sodium citrate, polyacrylamide, Iron(III) chloride hexahydrate, urea, 3-amino-propyltriethoxysilane (APTES), glutaraldehyde, and Tween 20 were purchased from Aldrich (St. Louis, Missouri) and were used without further purification. Deionized water (18.3 MΩ cm^{-1}) was obtained using a reverse osmosis water purification system and was used to prepare the phosphate buffer (PB) solution. Monoclonal *Salmonella* antibody and goat anti-mouse IgG antibody were purchased from Abcam Inc. (Cambridge, Massachusetts).

Synthesis of antibody-functionalized magnetic nanoparticle clusters (MNCs). Fe_3O_4 magnetic nanoparticle clusters were synthesized using a hydrothermal method, as described elsewhere[32]. Briefly, 4 mM $FeCl_3$, 8 mM sodium citrate and 12 mM urea were added to 80 mL DI water. After mixing the solution for 1 min, 0.6 mM polyacrylamide was added under vigorous stirring at room temperature. The solution was gradually heated to 200°C in a Teflon-lined autoclave and maintained for 10 h. The resulting MNCs were magnetically separated and rinsed a few times with DI water and absolute ethanol. The surfaces of MNCs were treated with 1% APTES in ethanol and 0.5% glutaraldehyde in water, then 10 μg of goat anti-mouse IgG antibody was immobilized onto the MNCs as a linker to produce oriented immobilization of the *Salmonella* antibody. After passivating the surface of MNCs with 1 wt% Tween 20 in PB, 10 μg of the *Salmonella* antibody was immobilized.

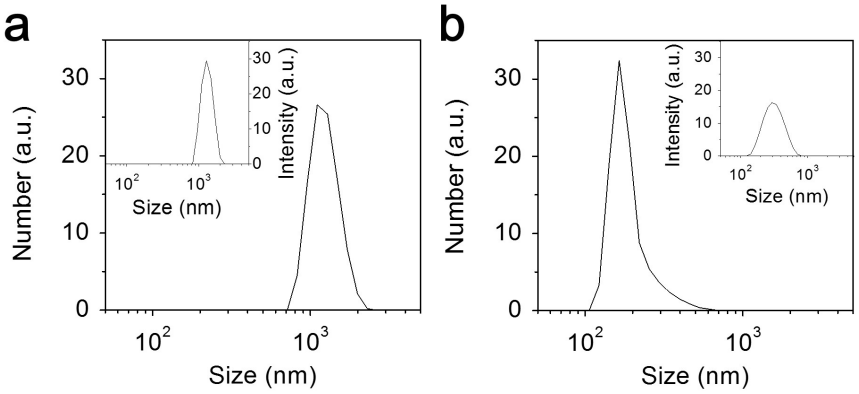

Figure 4 | DLS number mean size distribution curves of the solution (a) at the inner outlet, and (b) at the outer outlet. Intensity mean size distribution curves are shown as insets.

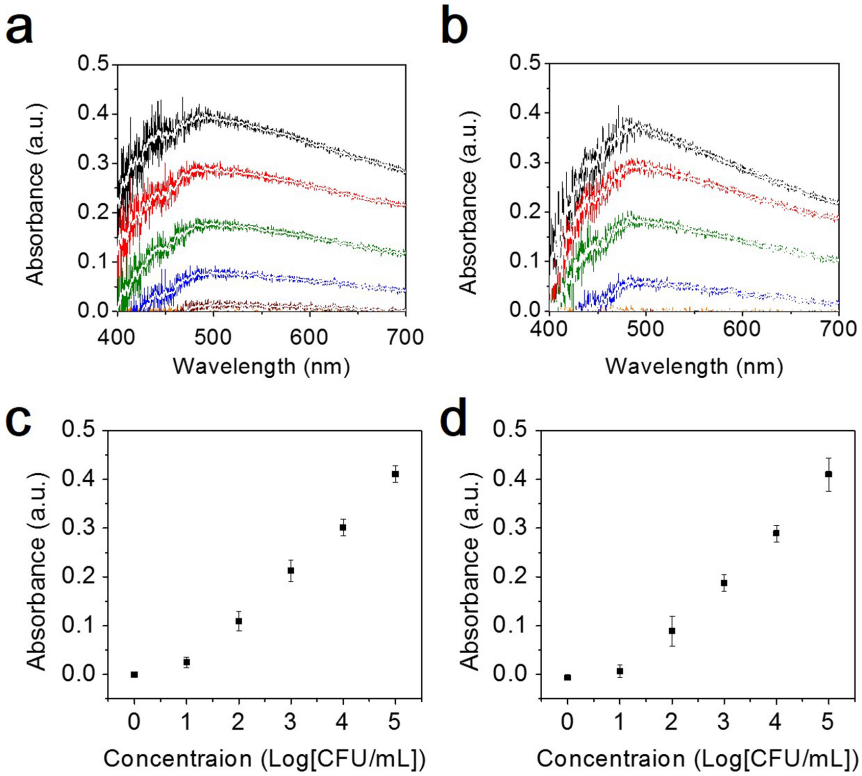

Figure 5 | UV-Visible absorbance spectra of the inner outlet MNC-EC samples having a range of concentrations in (a) buffer and (b) milk samples. The spectrum from top to bottom represents *E. coli* concentrations of 10^5 cfu/mL (black), 10^4 cfu/mL (red), 10^3 cfu/mL (green), 10^2 cfu/mL (blue), 10 cfu/mL (brown), and 0 cfu/mL (orange). Variations in the light absorption intensities of the solution at 484.9 nm for (c) buffer and (d) milk samples.

Fabrication of the microfluidic device. The three-dimensional microfluidic device containing a helical microchannel with trapezoidal cross-section was fabricated using stereolithography as described elsewhere[26,33]. The device design was drafted using a 3D CAD software, Autodesk Inventor (San Rafael, California). The inner and outer heights of the channel with trapezoidal cross-section were designed to be 250 μm and 500 μm, respectively. The width of the channel cross-section was 1000 μm. The device consists of two inlets, two outlets, and a 10-loop helical microchannel with a radius of 1.5 cm. The pitch of the helical channel is 1 mm. The device was 3D-printed by FineLine Prototyping, Inc. (Raleigh, North Carolina) using a 3D Systems Viper SL system (Rock Hill, South Carolina) in High-Resolution Mode with a natural finish. DSM Somos® WaterShed XC 11122 (Heerlen, Netherlands) was selected as the resin due to its transparency and water resistance.

Capture and separation of *E. coli* bacteria. *E. coli*-spiked samples were prepared at concentrations in the range of 10 to 10^5 cfu/mL in either PB buffer or milk; 100 μL of antibody-functionalized MNCs (100 μg/mL) were added to 10 mL of *E. coli*-spiked samples and incubated for 1 h at room temperature with gentle shaking. The MNC-EC complexes and free MNCs were magnetically separated using a permanent magnet, rinsed with buffer solution, then resuspended in 5 mL of PB buffer. The solution was injected into the microfluidic device with or without a sheath flow for separation of MNC-EC complexes. The flow rates for the sample inlet or buffer sheath flow were both fixed at 5 mL/min. The actual device has built-in luer lock connector that is not shown in Figure 2(a) for better presentation purposes. Syringe pumps were used to introduce constant flow in the channel through the luer lock connection and tubing.

Size distribution measurements. Samples obtained from the outlets were magnetically concentrated and resuspended in 1 mL PB buffer solution for DLS measurements. Size distributions of free MNCs and MNC-EC complexes were determined using DLS measurements. Scattered light in the sample was detected and analyzed by using a Zetasizer (Malvern Instruments Ltd., England) with a He-Ne laser at a detection angle of 173°.

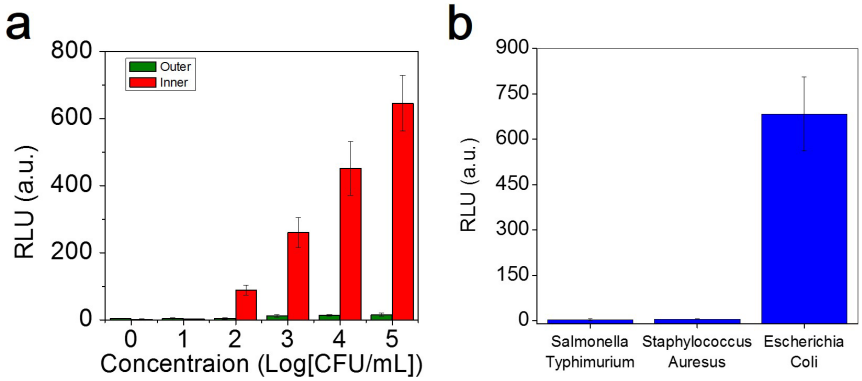

Figure 6 | (a) The intensities of the ATP luminescence measured for the inner outlet (red) and outer outlet (green) solutions after the injection of a milk solution spiked with different concentrations of *E. coli* bacteria. Concentrations of the control samples that are not spiked with bacteria were labeled "0" for convenience. (b) The intensities of the ATP luminescence, measured for the inner outlet solution after the injection of different bacteria at concentration of 10^5 cfu/mL at the inner outlet.

Bioluminescence measurements. The samples of MNC-EC complexes obtained from the inner outlet and outer outlet of the microfluidic device were magnetically concentrated to 50 μL and added to 150 μL of benzalkonium chloride solution to extract ATP from *E. coli* bacteria[29]. The ATP-extracted solution was sequentially added to lyophilized luciferin and luciferase powder, and the luminescence intensity was measured using a portable luminometer (Kikkoman PD-20). The photochemical reaction mechanism is described elsewhere[34,35]. In brief, luciferase catalyzed the adenylation of luciferin by ATP to form an intermediate, luciferyl adenylate, which is instantly oxidized by oxygen in solution to generate excited oxyluciferin. Finally, the excited oxyluciferin emits light while decaying to a stable state. Each ATP luminescence measurement was completed within 1 min.

1. Leonard, P. *et al*. Advances in biosensors for detection of pathogens in food and water. *Enzyme Microb. Technol.* **32**, 3–13 (2003).
2. Hobson, N. S., Tothill, I. & Turner, A. P. F. Microbial detection. *Biosens. Bioelectron.* **11**, 455–477 (1996).
3. Deisingh, A. K. & Thompson, M. Strategies for the detection of Escherichia coli O157: H7 in foods. *J. Appl. Microbiol.* **96**, 419–429 (2004).
4. Rodríguez-Lázaro, D. *et al*. A novel real-time PCR for Listeria monocytogenes that monitors analytical performance via an internal amplification control. *Int. J. Food Microbiol.* **101**, 93–104 (2005).
5. Shen, Z.-Q. *et al*. QCM immunosensor detection of Escherichia coli O157:H7 based on beacon immunomagnetic nanoparticles and catalytic growth of colloidal gold. *Biosens. Bioelectron.* **26**, 3376–3381 (2011).
6. Vaughan, R. D., O'Sullivan, C. K. & Guilbault, G. G. Development of a quartz crystal microbalance (QCM) immunosensor for the detection of Listeria monocytogenes. *Enzyme Microb. Technol.* **29**, 635–638 (2001).
7. Taylor, A. D. *et al*. Quantitative and simultaneous detection of four foodborne bacterial pathogens with a multi-channel SPR sensor. *Biosens. Bioelectron.* **22**, 752–758 (2006).
8. Torun, Ö., Hakkı Boyacı, İ., Temür, E. & Tamer, U. Comparison of sensing strategies in SPR biosensor for rapid and sensitive enumeration of bacteria. *Biosens. Bioelectron.* **37**, 53–60 (2012).
9. Ruan, C., Yang, L. & Li, Y. Immunobiosensor chips for detection of Escherichia c oli O157: H7 using electrochemical impedance spectroscopy. *Anal. Chem.* **74**, 4814–4820 (2002).
10. Jarvis, R. M. & Goodacre, R. Characterisation and identification of bacteria using SERS. *Chem. Soc. Rev.* **37**, 931–936 (2008).
11. Premasiri, W. R. *et al*. Characterization of the surface enhanced Raman scattering (SERS) of bacteria. *J. Phys. Chem. B* **109**, 312–320 (2004).
12. Disney, M. D., Zheng, J., Swager, T. M. & Seeberger, P. H. Detection of bacteria with carbohydrate-functionalized fluorescent polymers. *JACS* **126**, 13343–13346 (2004).
13. Gao, J. *et al*. Combining fluorescent probes and biofunctional magnetic nanoparticles for rapid detection of bacteria in human blood. *Adv. Mater.* **18**, 3145–3148 (2006).
14. Kim, U. & Soh, H. T. Simultaneous sorting of multiple bacterial targets using integrated Dielectrophoretic–Magnetic Activated Cell Sorter. *Lab Chip* **9**, 2313–2318 (2009).
15. Lee, J.-J. *et al*. Synthetic ligand-coated magnetic nanoparticles for microfluidic bacterial separation from blood. *Nano Lett.* **14**, 1–5 (2013).
16. Shim, W.-B., Song, J.-E., Mun, H., Chung, D.-H. & Kim, M.-G. Rapid colorimetric detection of Salmonella typhimuriumusing a selective filtration technique combined with antibody–magnetic nanoparticle nanocomposites. *Anal. Bioanal. Chem.* **406**, 859–866 (2014).
17. Mach, A. J. & Di Carlo, D. Continuous scalable blood filtration device using inertial microfluidics. *Biotechnol. Bioeng.* **107**, 302–311 (2010).
18. Hou, H. W. *et al*. Isolation and retrieval of circulating tumor cells using centrifugal forces. *Sci. Rep.* **3**, 1259 (2013).
19. Park, J.-S. & Jung, H.-I. Multiorifice flow fractionation: continuous size-based separation of microspheres using a series of contraction/expansion microchannels. *Anal. Chem.* **81**, 8280–8288 (2009).
20. Skowronek, V., Rambach, R. W., Schmid, L., Haase, K. & Franke, T. Particle Deflection in a Poly (dimethylsiloxane) Microchannel Using a Propagating Surface Acoustic Wave: Size and Frequency Dependence. *Anal. Chem.* **85**, 9955–9959 (2013).
21. Di Carlo, D., Irimia, D., Tompkins, R. G. & Toner, M. Continuous inertial focusing, ordering, and separation of particles in microchannels. *Proc. Natl. Acad. Sci. U.S.A.* **104**, 18892–18897 (2007).
22. Inglis, D. W., Davis, J. A., Austin, R. H. & Sturm, J. C. Critical particle size for fractionation by deterministic lateral displacement. *Lab Chip* **6**, 655–658 (2006).
23. Bhagat, A. A. S., Kuntaegowdanahalli, S. S. & Papautsky, I. Continuous particle separation in spiral microchannels using dean flows and differential migration. *Lab Chip* **8**, 1906–1914 (2008).
24. Martel, J. M. & Toner, M. Inertial focusing dynamics in spiral microchannels. *Phys. of Fluids* **24**, 032001 (2012).
25. Martel, J. M. & Toner, M. Particle focusing in curved microfluidic channels. *Sci. Rep.* **3**, 3340 (2013).
26. Au, A. K., Lee, W. & Folch, A. Mail-order microfluidics: evaluation of stereolithography for the production of microfluidic devices. *Lab Chip* **14**, 1294–1301 (2014).
27. Comina, G., Suska, A. & Filippini, D. Low cost lab-on-a-chip prototyping with a consumer grade 3D printer. *Lab Chip* **14**, 2978–2982 (2014).
28. Wu, L., Guan, G., Hou, H. W., Bhagat, A. A. S. & Han, J. Separation of leukocytes from blood using spiral channel with trapezoid cross-section. *Anal. Chem.* **84**, 9324–9331 (2012).
29. Asmolov, E. S. The inertial lift on a spherical particle in a plane Poiseuille flow at large channel Reynolds number. *J. Fluid Mech.* **381**, 63–87 (1999).
30. Warkiani, M. E. *et al*. Slanted spiral microfluidics for the ultra-fast, label-free isolation of circulating tumor cells. *Lab Chip* **14**, 128–137 (2014).
31. Dutz, S., Hayden, M. E., Schaap, A., Stoeber, B. & Häfeli, U. O. A microfluidic spiral for size-dependent fractionation of magnetic microspheres. *J. Magn. Magn. Mater.* **324**, 3791–3798 (2012).
32. Joo, J. *et al*. The facile and sensitive detection of pathogenic bacteria using magnetic nanoparticles and optical nanocrystal probes. *Analyst* **137**, 3609–3612 (2012).
33. Lee, W. *et al*. Ultra-rapid detection of pathogenic bacteria using a 3d immunomagnetic flow assay. *Anal. Chem.* **86**, 6683–6688 (2014).
34. Ito, K., Nishimura, K., Murakami, S., Arakawa, H. & Maeda, M. Novel bioluminescent assay of pyruvate phosphate dikinase using firefly luciferase–luciferin reaction and its application to bioluminescent enzyme immunoassay. *Anal. Chim. Acta* **421**, 113–120 (2000).
35. Qiu, J., Zhou, Y., Chen, H. & Lin, J.-M. Immunomagnetic separation and rapid detection of bacteria using bioluminescence and microfluidics. *Talanta* **79**, 787–795 (2009).

Acknowledgments

This work was supported by the National Research Foundation of Korea (NRF) grant funded by the Korea government (MEST) (No.2014R1A2A2A01007027). W.L. acknowledges the grant from POSTECH Presidential Fellowship.

Author contributions

W.L. designed, carried out the experiments, collected and analyzed the data, and wrote the manuscript; D.K. and W.C. helped with experiments and data analysis; G.Y.J. helped with data analysis; S.J. conceived the experiments, analyzed results, and wrote the manuscript.

Additional information

Competing financial interests: The authors declare no competing financial interests.

How to cite this article: Lee, W., Kwon, D., Choi, W., Jung, G.Y. & Jeon, S. 3D-Printed Microfluidic Device for the Detection of Pathogenic Bacteria Using Size-based Separation in Helical Channel with Trapezoid Cross-Section. *Sci. Rep.* **5**, 7717; DOI:10.1038/srep07717 (2015).